International Journal of Biological Macromolecules 268 (2024) 131871

Contents lists available at ScienceDirect

International Journal of Biological Macromolecules

journal homepage: www.elsevier.com/locate/ijbiomac

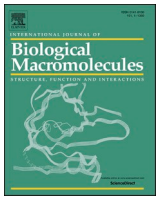

Quaternary ammonium carboxymethyl chitosan composite hydrogel with efficient antibacterial and antioxidant properties for promoting wound healing

Yahao Ma [1], Xujie Zhou [1], Zhendong Mo, Qing Zhou, Bingyu Hui, Zhuangzhuang Cai, Xiaoying Wang [*], Hang Li [*], Shunqing Tang [*]

Key Laboratory of Biomaterials of Guangdong Higher Education Institutes, Department of Biomedical Engineering, College of Life Science and Technology, Jinan University, Guangzhou 510632, China

ARTICLE INFO

Keywords:
Hydrogel
Antibacterial
Adhesive
Antioxidant
Wound healing

ABSTRACT

Multifunctional hydrogels have been developed to meet the various requirements of wound healing. Herein, an innovative hydrogel (QCMC-HA-PEG) was formed through the Schiff base reaction, composed of quaternary ammonium-modified carboxymethyl chitosan (QCMC), hyaluronic acid (HA), and 8-arms Polyethylene Glycol aldehyde (8-ARM-PEG-CHO). The resulting hydrogels exhibited good mechanical and adhesive properties with improved antibacterial efficacy against both Gram-positive and Gram-negative bacteria compared to CMC hydrogels. QCMC-HA-PEG hydrogels demonstrated remarkable adhesive ability in lap-shear test. Furthermore, the incorporation of MnO_2 nanosheets into the hydrogel significantly enhanced its reactive oxygen species (ROS) scavenging and oxygen generation capabilities. Finally, experimental results from a full-thickness skin wound model revealed that the QCMC-HA-PEG@MnO_2 hydrogel promoted skin epithelization, collagen deposition, and inflammatory regulation significantly accelerated the wound healing process. Therefore, QCMC-HA-PEG@MnO_2 hydrogel could be a promising wound dressing to promote wound healing.

1. Introduction

Skin is the largest organ of the human body, protecting tissues and organs from harmful bacteria as well as physical and chemical damage. In case of injury, bacteria and other microbes could easily invade the body, disrupting the physiological balance and potentially leading to severe illness or even death in the worst situation [1–3]. When replacing the dressings, traditional wound dressings (like gauze) could easily adhere to newly regenerated soft tissue leading to secondary injury [4]. To effectively promote wound healing, the optimal wound dressings should have the following properties: 1) rapidly absorbing wound exudate and maintaining a proper healing environment; 2) creating an environment with adequate oxygen levels to expedite wound healing; 3) exhibiting good biocompatibility and having the ability to promote cell proliferation and migration [5–8]. Due to their good permeability, excellent biocompatibility, and ability to provide a moist environment, hydrogels have been widely used as wound dressings, which are mainly fabricated with natural polymers such as HA, sodium alginate (SA), and chitosan (CS) [9–11]. However, the functions of single-component hydrogel still have many limitations in practical applications [12–14].

Carboxymethyl chitosan (CMC), a derivative of CS, exhibits biocompatibility, biodegradability, and antibacterial activity. However, the antibacterial efficacy of CMC needs to be further enhanced in order to achieve the status of an ideal wound dressing [15]. Polymer quaternary ammonium salt has remarkable antibacterial activity and low toxicity, making it a research hotspot in the field of antibacterial agents [16,17].

In previous studies, Aiping Hui et al. developed an antibacterial material by incorporating quaternary ammonium chitooligosaccharides into the ZnO/palygorskite nanocomposite by self-assembly process, resulting in a nanocomposite with excellent antibacterial activity [18]. Inspired by this, in this study, QCMC was synthesized by grafting quaternary ammonium groups onto CMC via a nucleophilic substitution process. This approach allows QCMC to retain the inherent biological characteristics of CMC as a natural polysaccharide while harnessing the potent antibacterial properties of quaternary ammonium salts.

* Corresponding authors.
E-mail addresses: wangxi@jnu.edu.cn (X. Wang), hangli@jnu.edu.cn (H. Li), tshunqt@jnu.edu.cn (S. Tang).
[1] Contributed equally to this work.

https://doi.org/10.1016/j.ijbiomac.2024.131871
Received 18 August 2023; Received in revised form 29 March 2024; Accepted 23 April 2024
Available online 25 April 2024

The adhesive and anti-inflammatory abilities stand as pivotal characteristics of wound dressings. Hydrogel dressings with good adhesive ability can effectively adhere to wounds and are the premise for dressings to function normally in the human body part, particularly in joint parts [19]. As a main ingredient of the extracellular matrix, HA contributes to the movement and proliferation of cells and has anti-inflammatory properties. The carboxyl groups present in HA can form peptide bonds by linking with the amino groups found in tissues. Hence, HA was integrated into CMC to enhance its adhesive properties [9,20].

To improve the mechanical properties of the wound dressings, 8-ARM-PEG-CHO was incorporated into the crosslinking structure [21]. In our previous study, the multi-armed polyethylene glycol structure was introduced into chitosan hydrogel, and the mechanical properties of the hydrogel were significantly improved [22].

Excessive ROS can significantly delay the wound healing process [23]. As one of the efficient nanozymes, manganese dioxide (MnO_2) nanosheets could catalyze the decomposition of hydrogen peroxide to oxygen and water, reducing oxidative stress [24]. Compared with other nanoenzymes such as nanoceria (CeO_2), gold nanoclusters, and C_3N_4 nanofusiform, MnO_2 nanosheets are biodegradable and biocompatible [25]. Hence, the incorporation of MnO_2 nanosheets into QCMC-HA-PEG hydrogel enhances its capacity to scavenge ROS while concurrently generating oxygen, thereby fostering cell activity, promoting cell proliferation and migration, and ultimately expediting the wound healing process [26,27].

In this study, CMC was first modified by grafting strong positively charged quaternary ammonium salt groups onto CMC via nucleophilic substitution reaction, resulting in the formation of QCMC to enhance its antibacterial performance. To further improve the adhesive and mechanical capability of the hydrogel, HA and 8ARM-PEG-CHO were added to QCMC, forming a double cross-linking network. MnO_2 nanosheets were uniformly dispersed within QCMC-HA-PEG hydrogels (QCMC-HA-PEG@MnO_2) (Fig. 1) further enhancing ROS scavenging ability and generating O_2. Compared to previously published studies focusing on individual properties, our synthesized hydrogel exhibits comprehensive characteristics [12–14]. It is hypothesized that the QCMC-HA-PEG@MnO_2 hydrogel could regulate inflammation promote angiogenesis and re-epithelialization, accelerate collagen deposition, and effectively facilitate skin wound healing and tissue restoration.

2. Materials and methods

CMC (M_W = 100–200 kDa, degree of substitution≥80 %) and HA (400–1000 kDa) were obtained from Shanghai Yuanye Bio-Technology Co., Ltd. 8ARM-PEG-CHO (10 kDa) was obtained from Guangzhou Tanshtech Bio-Technology Co., Ltd. Calcein-AM/PI, and hematoxylin-eosin were obtained from Jiangsu Keygen Biotech Co., Ltd. Masson's trichrome was obtained from Wuhan Service Co., Ltd. DMEM was purchased from BioChannel Biological Technology Co., Ltd.Fetal Bovine Serum (FBS) was offered by CellMax cell Technology (Beijing) Co., Ltd. Cell Counting Kit-8 (CCK-8) was offered by Solarbio (Beijing, China). Cell flow cytometry analysis was performed using Challenbio's LongCyto™ detection. RT SuperMix for qPCR was offered by Novoprotein, Shanghai, China. Cell culture dishes was purchased from NEST Biotechnology Co., Ltd. All other reagents were of analytical grade and were used directly without further preparation.

2.1. Preparation of QCMC-HA-PEG@MnO_2 hydrogels

The CMC solution was prepared by dissolving 1 g of CMC in 25 mL of

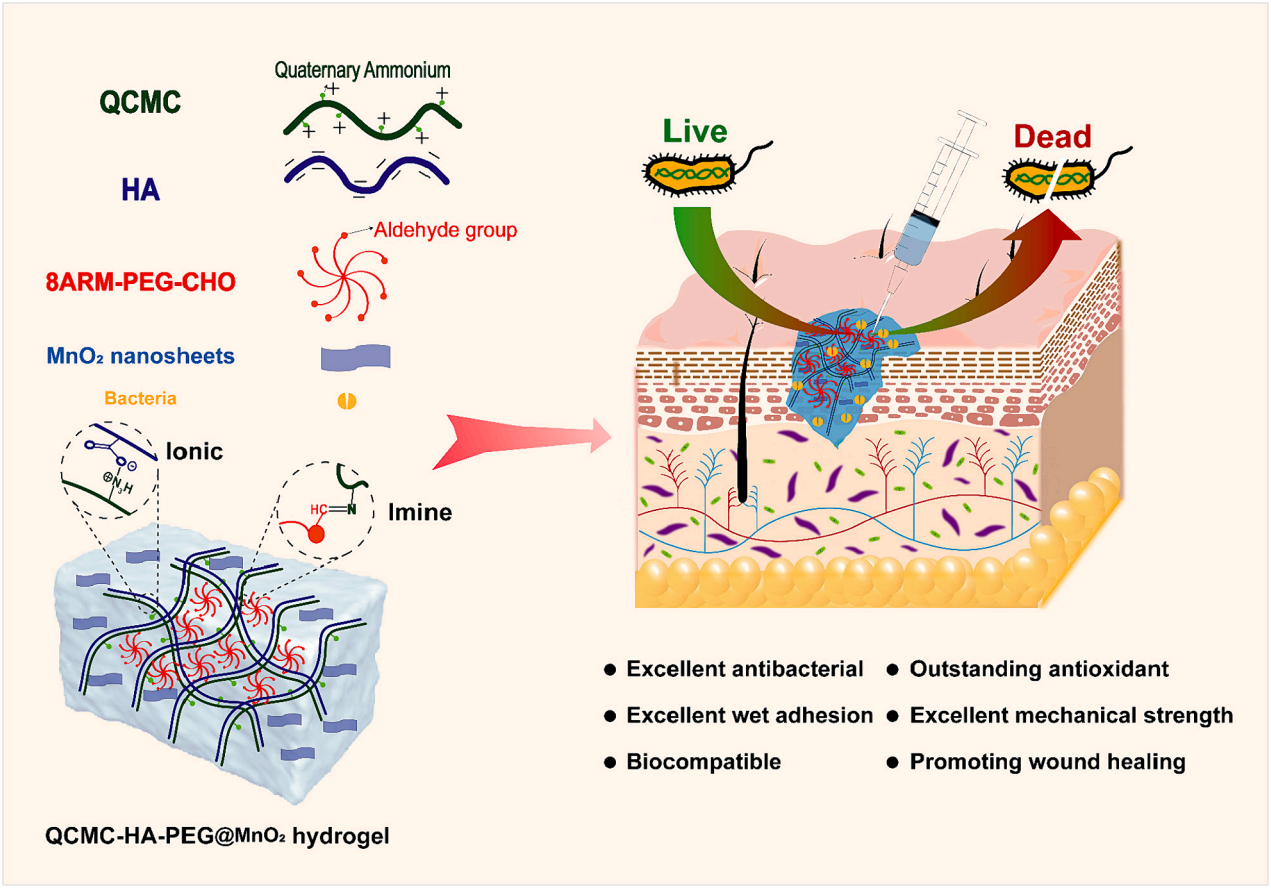

Fig. 1. Schematic of the preparation of QCMC-HA-PEG@MnO_2 hydrogel with multifunctional properties including antibacterial, antioxidant, and promoting wound healing capabilities.

deionized water, followed by dropwise addition of solutions containing 1 mmol, 2 mmol, and 3 mmol of GTA to synthesize 1QCMC, 2QCMC, and 3QCMC. Then the solution was placed in an oil bath at 65 °C and reacted for 14 h. After that, anhydrous ethanol was added to the solution, centrifuged, and the bottom product was redissolved in deionized water and dialyzed against DI water for 2 days (change water 3 times a day). The final solution was freeze-dried and product was stored for further use.

To prepare CMC-PEG hydrogels, 300 μL of a 5 wt% CMC solution and 20 μL of an 8ARM-PEG-CHO (molar ratio 1:1) solution were fully mixed and formed hydrogel within 5 min.

To prepare 1QCMC-HA-PEG hydrogel, 300 μL of 1QCMC solution (5 wt%) was fully mixed with 100 μL of HA solution (1.5 wt%). Next, 20 μL 8ARM-PEG-CHO (100 mg/mL) was added and fully mixed. The hydrogel could be formed within 5 min. 2QCMC-HA-PEG and 3QCMC-HA-PEG hydrogels were prepared following the same procedure.

To prepare δ-MnO_2, 2.2 g of TMAOH-5H_2O was dissolved in 20 mL of 3 wt% H_2O_2 with stirring, and 0.594 g of $MnCl_2$-4H_2O was dissolved in 10 mL of deionized water using sonication. The TMAOH solution was added to the $MnCl_2$ solution and stirred for 12 h, and the final solution was centrifuged at 4230 rpm for 5 min. MnO_2 was obtained at the bottom of the centrifuge tube, which was then subjected to three washes with deionized water and dried using a vacuum dryer to obtain the final MnO_2 nanosheets. To prepare the QCMC-HA-PEG@MnO_2 hydrogel rich in nanoenzyme, different concentrations of MnO_2 nanosheets were added to QCMC-HA-PEG.

2.2. Characterization of hydrogels

The morphology of hydrogel and the MnO_2 nanosheets were characterized by Scanning Electron Microscopy (SEM) and Transmission Electron Microscope (TEM).

The chemical structures of the materials (selecting the 2QCMC as a representative) were characterized by Fourier Transform Infrared Spectroscopy (FTIR) spectrometer and 500 MHz Nuclear Magnetic Resonance (NMR) spectroscopy. Using an X-ray diffractometer (XRD), the hydrogel's phase structure was examined. The EA2400II elemental analyzer was employed to determine the percentage content of carbon (C), hydrogen (H), and nitrogen (N) elements within the hydrogel.

The distribution of MnO_2 nanosheets particle sizes was assessed using a nanoscale analyzer. Additionally, high-resolution spectra of Mn 2p and O 1 s were obtained for the MnO_2 samples using a 40 eV electron energy analyzer.

The viscoelastic properties and gelation time (s) of hydrogels were tested by rheometer. Strain tests were carried out with a strain of 1 %, a frequency of 1 Hz, and a temperature of 25 °C to evaluate the storage modulus (G′) and loss modulus (G″) of the hydrogel.

For the hydrogel swelling test, hydrogels were first freeze-dried weighed (W_0), and then placed into PBS. At certain time intervals, the hydrogels were taken out and reweighed (W_t). The swelling ratio SR (g/g), was determined for each batch of hydrogels using the following formula:

$$SR(g/g) = \frac{W_t - W_0}{W_0}$$

2.3. Hydrogel adhesion and self-healing properties test

The lap-shear test was performed to investigate the adhesive ability of hydrogel. The fresh pig skin was sliced into rectangular pieces measuring 2 × 5 cm^2. Subsequently, the freshly prepared hydrogel was applied onto the pig skin, and its adhesive performance was assessed through shear strength tests [22]. The tests were performed in triplicates. To observe the self-healing process, two hydrogels were stained with different food colors (green and orange) and then cut in half. The cutting pieces were put together and recording the time for them to heal together completely.

2.4. Antibacterial assay

The antibacterial activity of the hydrogel was assessed using *E. coli* (ATCC® 35320™) and *S. aureus* (ATCC 6538P). All materials underwent sterilization using ultraviolet light for 6 h before the experiment. Subsequently, the hydrogels were positioned in 24-well plates, which were then added with 990 μL of LB broth and 10 μL of *E. coli* or *S. aureus* at a concentration of 1×10^7 CFU/mL, well-mixed. In the control group, no treatment was administered to the 24-well plates, which were subsequently incubated in a biochemical incubator at 37 °C for 24 h.

PBS solution was used to dilute the bacterial solution in the 24-well plate to a concentration of 100 CFU/mL, and 100 μL of the dilute bacterial droplets were then introduced and equally distributed on the surface of the AGAR medium. After being cultured in the biochemical incubator at 37 °C for 24 h, the number of colonies on the AGAR dish was recorded using a digital camera. The following formulas are used to calculate the bacterial survival rate (V) and antibacterial rate (R):

$$V(\%) = \frac{N_{Sample}}{N_{Control}} \times 100\%$$

$$R(\%) = 1 - V(\%)$$

where N_{Sample} is the number of colonies in the material group and $N_{Control}$ is the number of colonies in the empty control group.

2.5. ROS scavenging and oxygen generation assays

Using the o-diazepine-Fe^{2+} oxidation technique, the hydroxyl (·OH) free radical's scavenging capacity was measured [28]. The sample solution to be tested was prepared by mixing 2 mL H_2O_2 solution (100 μM) with 2QCMC-HA-PEG@MnO_2 hydrogel with different concentrations of MnO_2 nanosheets contents (0.1 %, 0.05 %, 0.025 %). 500 μL $FeSO_4$ solution (9 mM), 1 mL salicylic acid-ethanol solution (9 mM), 2 mL deionized water and 1 mL sample solution to be tested were mixed and incubated in an incubator at 37 °C for 1 h. The solution's absorbance (510 nm) was measured with a plate reader. 2QCMC-HA-PEG@MnO_2 hydrogel (500 μL) was added into 1 mL H_2O_2 solution (100 μM), and the O_2 concentration was detected by a commercial oxygen meter (PreSens, OXY-1 ST Trace) according to the manufacturer's instructions [25].

2.6. Cytotoxicity test

The cytotoxic activity of hydrogels was assessed using mouse embryonic fibroblasts (NIH3T3). NIH3T3 cells were seeded in well plates at a density of 3000 cells per well, and 200 μL of culture medium (high glucose DMEM medium, 10 % fetal bovine serum, and 2 % pen/strep) was added. The cells were then grown at 37 °C in a cell incubator [22]. Once the cells adhering to the surface of the culture flask, the initial media was replaced with media solution containing hydrogel extract solution. The sample solutions were removed on day 1, day 2, and day 3, and the wells were washed twice with PBS.

On day 1, day 2, and day 3, NIH3T3 cell viability was analyzed using the LIVE/DEAD cell viability assay following previous studies and the manufacturer's protocol [22]. After that, photographs were taken with an inverted fluorescence microscope (MF53-N, Mingmei, Guangzhou, China).

2.7. In vivo wound healing

Female Sprague Dawley (SD) rats weighing approximately 180–220 g were used to evaluate the in vivo wound healing ability of the hydrogels. The animal experimental procedures were performed according to the Guidelines for National Research Council's Guide for the

Care and Use of Laboratory Animals and approved by the Animal Ethics Committee of Jinan University (2020031845). The wound was created with a biopsy punch on the back of rats (wound position was illustrated in Fig. S10), and treated with different materials control (no treatment), CMC-HA-PEG, 2QCMC-HA-PEG, and 2QCMC-HA-PEG@MnO_2. On days 0, 3, 7, and 14, the wound size was captured using a digital camera, and the closure rate was quantified. Additionally, the skin tissues of surgical areas were collected for further investigation on days 3, 7, and 14 respectively.

2.8. Analysis of immune infiltration in wound tissue

On day 14, the skin tissue was ground and filtered through a 200-mesh copper mesh to obtain a tissue suspension, which was then centrifuged at 2000 rpm for 5 min to collect the cells. To assess M2 macrophage infiltration in skin tissue, the collected cells were incubated with macrophage flow cytometry antibodies (Anti-CD11b-FITC, Anti-CD80-APC, and Anti-CD206-PE) for 30 min, and then centrifuged at 2000 rpm for 5 min to remove the unbound antibodies. After washing once with PBS (0.01 M, pH = 7.4), the stained cells were resuspended with 500 μL of PBS and analyzed by flow cytometry [29].

2.9. Histopathological analysis and quantitative PCR

The skin samples, including the wound area and its surrounding tissue, were collected and preserved in a 4 % paraformaldehyde solution before embedding in paraffin. Following this, the tissue samples underwent sectioning, dewaxing, staining, and histopathological assessment. Staining techniques include Hematoxylin and Eosin (H&E) staining and Masson's trichrome staining. The images were captured using an inverted microscope (MF53-N, Mingmei, Guangzhou, China). Quantitative PCR (qPCR) steps in supplementary materials [30].

2.10. Imaging and analysis

The thickness of the epidermis was measured using Image J software. The degree of collagen deposition is calculated as the collagen index: (B + G)/(2R + B + G) for each pixel in the image (R, B, and G represent red, blue, and green pixel values, respectively) [31]. The collagen index ranges from 0 to 1 (meaning that the subject is extremely red to completely turquoise).

2.11. Statistical analysis

All data are shown as the mean standard deviation of at least three independent experiments. Significant was tested by student *t*-test (ANOVA). Statistical analysis was performed using JMP Pro 13 software (SAS Institute, Cary, North Carolina, USA) [32].

3. Results and discussion

3.1. Characterization of hydrogels

The hydrogen NMR spectra of CMC and QCMC are shown in Fig. 2A. The peak at 4.23 ppm in the CMC spectrum was attributed to the proton on the carboxymethyl [33]. Another strong signal at 3.15 ppm corresponds to the proton of the methyl in the quaternary ammonium salt. The proton signal in the chain of the quaternary ammonium salt was at 2.71 ppm, 4.10 ppm, and 3.33 ppm [34]. The results confirmed that the quaternary ammonium salt was successfully grafted onto CMC.

The FTIR spectra of CMC and QCMC were shown in Fig. 2B. In the infrared spectrum of QCMC, the peak of 3439 cm^{-1} was shifted to 3257 cm^{-1}, which was due to the reaction of the amino groups in CMC and the breaking of hydrogen bonds [35]. Moreover, it was identified that the presence of the trimethyl quaternary ammonium ion led to the appearance of a novel absorption peak at 1476 cm^{-1}. In the infrared spectrum of QCMC-HA-PEG, the absorption peaks near 1047 cm^{-1} are attributed to the C-OH bonds in HA, proving that HA is involved in the formation of double-network hydrogels. This result demonstrates the successful synthesis of double-network hydrogels (Fig. S1) [36].

The XRD patterns of CMC and QCMC were shown in Fig. 2C. CMC exhibited strong diffraction absorption peaks at 2θ = 10.62° and 19.9°, indicating that CMC had a crystal structure. Except for the weak diffraction absorption peak at 2θ = 20°, the diffraction peaks in other parts of QCMC disappeared. After the quaternization of CMC, the content of free amino groups in the molecular chain decreased, leading to a decrease in the number of hydrogen bonds in the macromolecular chain and thus a decrease in crystallinity. Furthermore, the introduction of quaternary ammonium salt groups into CMC molecules weakened the hydrogen bonding between CMC molecules and destroyed the crystal structure [34]. Hence, the XRD results confirmed the amorphous nature of carboxymethyl chitosan as a polymer. Additionally, to validate the successful synthesis of CMC from the quaternary ammonium salt and to

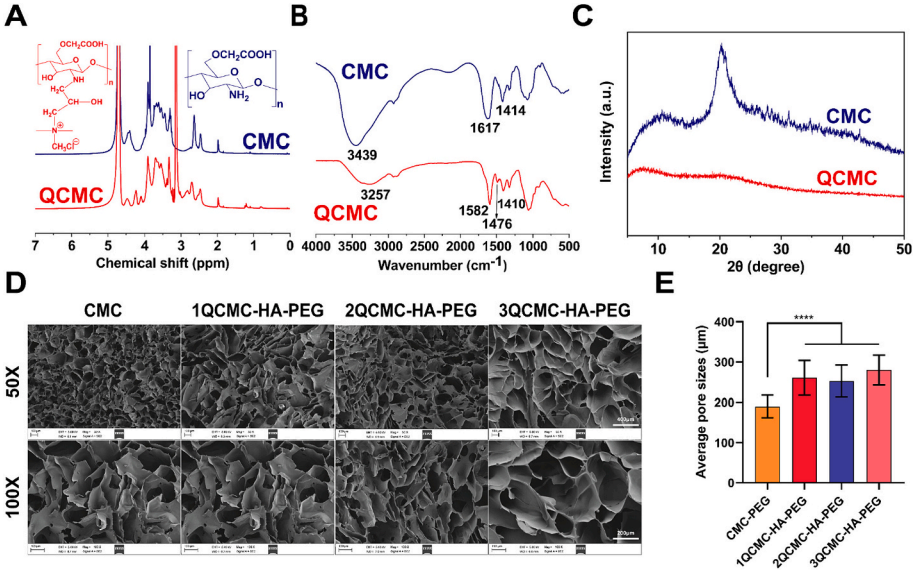

Fig. 2. (A) ^{1}H NMR spectra of QCMC and CMC; (B) FTIR spectra of QCMC and CMC; (C) X-ray diffraction pattern of QCMC and CMC; (D) microstructure of different hydrogels imaged by SEM; (E) average pore sizes of different hydrogels. ($n = 3$, $^{****}p < 0.0001$.)

ascertain the degree of substitution (DS) of QCMC, the elemental analysis results of each raw material and product were presented in Table S1. These findings demonstrated that the DS of substitution of the quaternary ammonium salt in QCMC increased with the rise in the reactant GTA.

As shown in Fig. 2D, all hydrogel samples had a relatively uniform three-dimensional interconnected pore structure, which promoted the penetration and transfer of nutrients and oxygen on the wound surface. The pore size of CMC-PEG hydrogel was the smallest (189.7 ± 27.97 μm). The pore sizes of 1QCMC-HA-PEG, 2QCMC-HA-PEG, and 3QCMC-HA-PEG hydrogels were 260.7 ± 43.17 μm, 252.6 ± 39.82 μm, and 280.2 ± 37.01 μm, respectively (Fig. 2E). Because grafting the quaternary ammonium salt onto CMC affects the formation of the Schiff base bond, resulted in a lower crosslink density of the hydrogels and thus lead to larger pore size.

The morphology of the prepared MnO_2 nanosheets was characterized by TEM. The MnO_2 nanosheets showed a layered structure (Fig. S2A). The particle size of the MnO_2 nanosheets was 375.45 nm (Fig. S2B). The binding energy of the 2QCMC-HA-PEG@MnO_2 composite hydrogel was the Mn 2p1/2 peak at 654.2 eV and the Mn 2p 3/2 peak at 642.4 eV, and the difference between the two is 11.7 eV (Fig. S2C). The existence of MnO_2 nanosheets was confirmed, and the significant O 1 s peak confirmed the existence of Mn(IV)O_2 nanosheets further (Fig. S2D) [37,38]. The above results demonstrate the successful preparation of MnO_2 nanosheets and their successful incorporation into the 2QCMC-HA-PEG hydrogel.

Fig. S3 shows that the hydrogel absorbed water and swelled rapidly after immersion in PBS. The swelling rate reached the maximum after about 30 min and reached equilibrium after 2 h. Among them, CMC-PEG hydrogel has the lowest swelling rate and reaches swelling equilibrium after swelling 19.6-fold. The swelling rates of the three hydrogels (1QCMC-HA-PEG, 2QCMC-HA-PEG, and 3QCMC-HA-PEG) were 27-fold, 30-fold, and 36-fold, respectively. This occurred because the hydrogels' swelling rates increased with decreasing crosslink density and increasing pore size.

3.2. Rheological properties of hydrogels

Fig. 3A shows the representative images of different hydrogel types. 3QCMC-HA-PEG hydrogels had difficulty forming a regular shape, so further studies focused on 1QCMC-HA-PEG and 2QCMC-HA-PEG. Compared with CMC-PEG, the gelation time of 1QCMC-HA-PEG, and 2QCMC-HA-PEG were 186 ± 24 s, and 241 ± 19 s, respectively (Fig. 3B). The higher the grafting ratio of the quaternary ammonium salt, the more amino groups were occupied on the CMC, resulting in a prolonged gelation time of the hydrogel. As shown in Fig. 3C–D, in the scan frequency range of 0.1–10 Hz, G′ of the hydrogels in all groups was larger than G″, indicating that they all had a stable gel network. At a sampling frequency of 10 Hz, the G′ values of the hydrogels CMC-PEG, 1QCMC-HA-PEG, and 2QCMC-HA-PEG were 145.7 Pa, 120.4 Pa, and 141.5 Pa, respectively. The energy storage modulus of 2QCMC-HA-PEG is similar to that of CMC-PEG, indicating that the modified hydrogel 2QCMC-HA-PEG also has good mechanical properties. Fig. S5 shows that hydrogels could maintain a stable network structure in the strain range of 0.01%~126%. When the strain reaches 126%, the curve of G′ intersects with that of G″, indicating the hydrogel has a gel-sol transition.

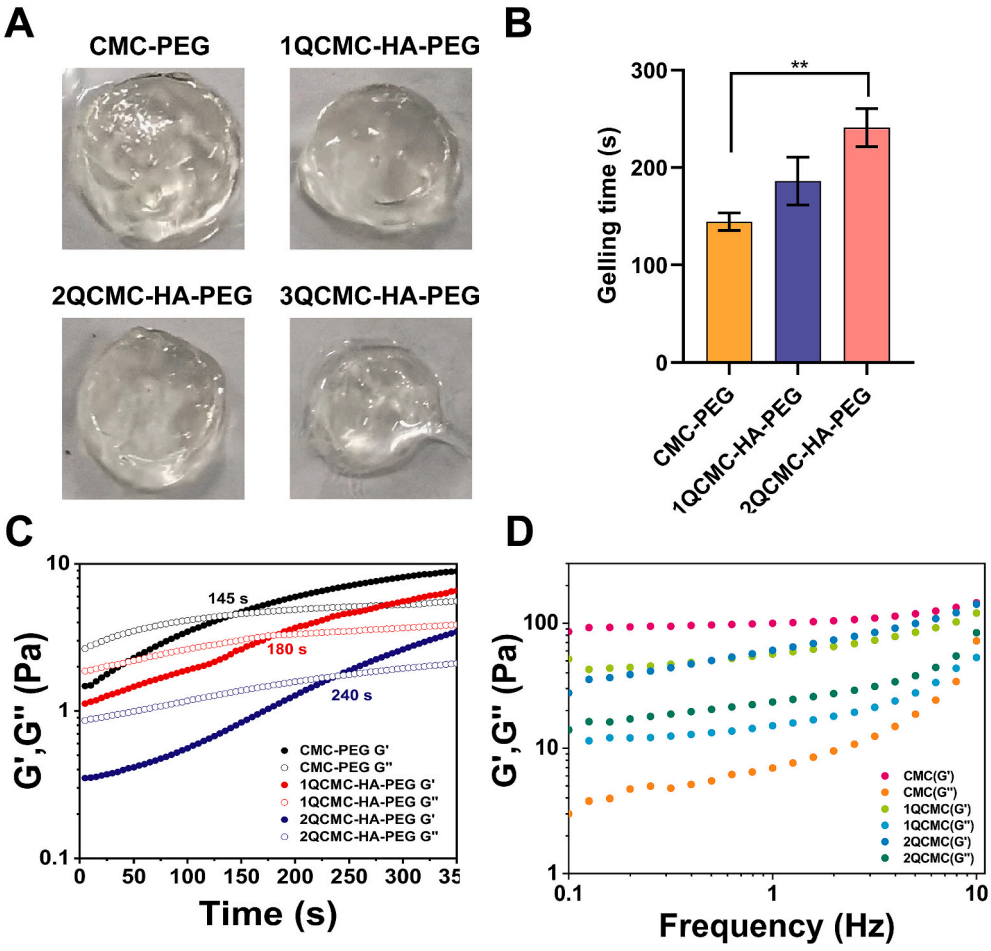

Fig. 3. (A) Representative images of different hydrogels; (B) gelling time of different hydrogels; (C) rheology dynamic time sweeps of different hydrogels; (D) frequency sweep analysis of different hydrogels. ($n = 3$, $^{**}p < 0.01$.)

After that, the value of G′ is higher than that of G″, demonstrating that the hydrogel network collapses and changes into a liquid state.

Moreover, for biomedical applications, the ideal hydrogel degradation rate is critical. On day 14, there was no significant difference between the groups in the remaining weights of the CMC-PEG, 2QCMC-HA-PEG, and 2QCMC-HA-PEG@MnO_2 hydrogels, which were 54.3 ± 2.3 %, 45.2 ± 6.8 %, and 51.6 ± 5.7 %.

3.3. Hydrogel adhesion and self-healing properties test

Fig. 4A illustrates the application of the QCMC-HA-PEG hydrogel on fresh porcine skin, demonstrating good adhesive ability between the hydrogel and skin. The hydrogel remained attaching to the porcine skin firmly, in the process of being subjected to bending, twisting, and flushing with tap water. The adhesive mechanism of hydrogel could be concluded as following: 1) the free negative-charged carboxyl groups can bind to the glycosyl compounds (glycolipids or glycoproteins) on the cell membrane of skin tissues, resulting in an adhesion effect [39]; 2) the existence interactions between materials and tissue surfaces, such as hydrogen bonding, hydrophilic and hydrophobic interactions. Fig. 4B mainly displays the relevant experimental parameters and methods of lap shear test. Fig. 4C shows that compared with CMC-PEG (1.05 ± 0.41 kPa) and 1QCMC-HA-PEG (5.35 ± 0.47 kPa) hydrogel, the adhesion strength of 2QCMC-HA-PEG hydrogel was higher (5.78 ± 0.12 kPa), showing excellent adhesion properties. The 2QCMC-HA-PEG hydrogel had a good adhesion effect on skin tissue, and the adhesion strength was higher than that of commercial fibrin gel (3.90 ± 0.42 kPa) [40].

To show the self-healing ability of QCMC-HA-PEG hydrogels, two hydrogels (with different colors) were cut in half. Subsequently, the two cut pieces were connected, and after 10 min, the two hydrogels could merge (Fig. S6). The excellent injectability of the hydrogel is further demonstrated in Fig. S7.

3.4. Antibacterial assay

The anti-bacterial ability of different hydrogels against *E. coli* (ATCC® 35,320™) and *S. aureus* (ATCC 6538P) was investigated. Fig. 5A shows that the number of colonies in the CMC-PEG hydrogel group was slightly reduced compared to the control group. The number of colonies in the QCMC-HA-PEG group was significantly lower than that in the control group ($P < 0.001$). Furthermore, it was observed that the number of colonies decreased with the increase in the substitution level of quaternary ammonium salt. This trend indicates that the introduction of quaternary ammonium salt effectively enhanced the antibacterial effect of CMC. Compared to unmodified CMC, the positive charge density of QCMC is increased, and then the strong cationic

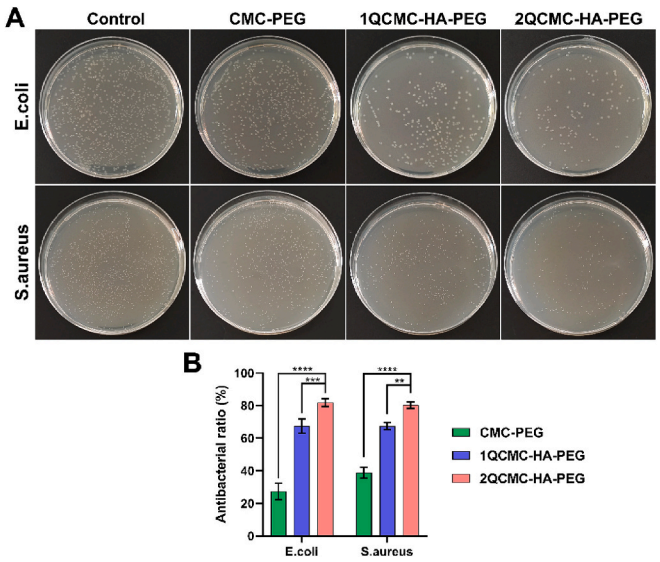

Fig. 5. (A) Representative images of the growth of bacterial colonies of *E. coli* and *S. aureus* on agar plates after co-culturing with hydrogels for 24 h; (B) the antibacterial ratio of hydrogels. ($n = 3$, $^{**}p < 0.01$, $^{***}p < 0.001$ and $^{****}p < 0.0001$.)

properties help it adsorb to negatively charged proteins and lipopolysaccharides on the surface of bacteria, leading to the death of bacteria [41]. As depicted in Fig. 5B, the antibacterial efficacy of the QCMC-HA-PEG hydrogel notably increased. The antimicrobial rates of the 2QCMC-HA-PEG group against *E. coli* and *S. aureus* were 81.85 ± 2.45 % and 80.25 ± 1.98 %, respectively.

The BCI value of both 1QCMC-HA-PEG and 2QCMC-HA-PEG hydrogels were notably lower compared to CMC-PEG. The RBC adsorption rate of both 1QCMC-HA-PEG and 2QCMC-HA-PEG hydrogels were notably higher compared to CMC-PEG. There was no significant distinction observed between the 1QCMC-HA-PEG and 2QCMC-HA-PEG hydrogels (Fig. S8). Nevertheless, the antibacterial efficacy of 2QCMC-HA-PEG surpassed that of 1QCMC-HA-PEG. Consequently, subsequent investigations were directed toward exploring the properties of 2QCMC-HA-PEG hydrogels. Fig. S9 shows the hemolysis rate of the hydrogel is <2 %, which is considered to be non-hemolytic. Therefore, all hydrogels have good blood compatibility.

3.5. ROS scavenging and oxygen generation assays

Excess ROS is one of the causes of delayed wound healing. The

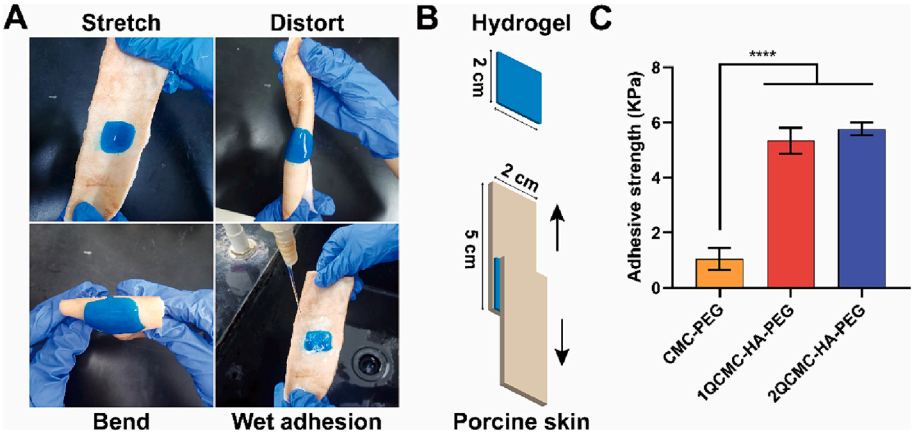

Fig. 4. (A) Photographs of hydrogels attached to the porcine skin; (B) schematic of the lap shear test; (C) the average adhesive strength of different hydrogels to the porcine skin. ($n = 3$, $^{****}p < 0.0001$.)

accumulation of ROS around the wound not only triggers a robust inflammatory response but also impairs the functions of skin fibroblasts, thus affecting the regeneration of wound tissue. However, the integration of MnO_2 nanosheets into the hydrogel not only effectively eliminates ROS but also promotes oxygen production around the wound area and stimulates cell growth [25].

Fig. 6A shows the successful synthesis of 2QCMC-HA-PEG@MnO_2 hydrogels with concentrations of 0.1 %, 0.05 %, and 0.025 % manganese dioxide. The oxygen probe was used to monitor oxygen concentration changes in the upper H_2O_2 solution (Fig. 6C). After 1 h of continuous monitoring, the oxygen release performance of hydrogel scaffolds with different concentrations of MnO_2 content was analyzed. As shown in Fig. 6B, the higher the concentration of MnO_2, the more oxygen was produced. After 40 min, the hydrogel containing 0.1 % MnO_2 reached a peak oxygen concentration of 91.48 %. Notably, both the 0.05 % and 0.025 % groups exhibited continued oxygen production even at the 60 min. Based on the test results, it was observed that the 0.025 % group exhibits a longer duration of oxygen release compared to the 0.05 % group. In addition, hydrogels with a concentration of 0.025 % MnO_2 exhibited more consistent oxygen production rates and longer oxygen release time. All three hydrogels exhibited good hydroxyl radical scavenging ability (Fig. 6D). The hydroxyl radical scavenging rates of 0.1 %, 0.05 %, and 0.025 % hydrogels were 40.83 ± 2.4 %, 32.34 ± 2.26 %, and 16.61 ± 2.88 %. Compared with other groups, the 0.025 %-2QCMC-HA-PEG@MnO_2 produced more uniform and persistent oxygen after eliminating the H_2O_2, which probably was attributed to the better dispersion of MnO_2 nanosheets. In summary, the 0.025 %-2QCMC-HA-PEG@MnO_2 nanosheets were chosen for subsequent experimental studies due to their ability to be evenly distributed and their prolonged oxygen production effect.

Furthermore, attaining optimal hydrogel degradation rates is paramount for biomedical applications. On day 14, the remaining weight of CMC-PEG and 2QCMC-HA-PEG hydrogels was measured to be 48.8 ± 0.86 % and 32.8 ± 0.8 %, respectively (Fig. S4). In comparison to CMC-PEG, it can be observed that 2QCMC-HA-PEG exhibits faster degradation performance, which may be attributed to the faster degradation rate of HA.

3.6. Cytotoxicity test

To further assess the impact of the three different hydrogels on cell proliferation, different hydrogel extract was cultured with NIH3T3 cells for three days. Fluorescence microscopy images in Fig. 7A revealed that the majority of cells were viable. The proliferation of the fibroblast cells demonstrated that the hydrogels did not induce cytotoxicity in the cells. In Fig. 7B, it is evident that on days 1, 2, and 3, the cell survival rate exceeded 95 % across all hydrogel groups, with no significant variance in cell viability observed between the different groups. Consequently, CMC-PEG, 2QCMC-HA-PEG, and 2QCMC-HA-PEG@MnO_2 hydrogels demonstrated minimal cytotoxicity to NIH3T3 cells and exhibited excellent cytocompatibility.

3.7. Evaluation of in vivo wound healing

The wound healing efficacy of CMC-PEG, 2QCMC-HA-PEG, and 2QCMC-HA-PEG@MnO_2 hydrogels was assessed through full-thickness wound-repair experiments. The wound healing progress was monitored over 14 days using a digital camera, and quantitative analysis of the wound area was conducted using Image J.

As the results show, the wound healing rate in the 2QCMC-HA-PEG@MnO_2 hydrogel group was faster than those in the CMC-PEG and 2QCMC-HA-PEG groups, according to the results of macroscopic examination images (Fig. 8A) and quantitative data (Fig. 8B–C). On day 3, the wound closure rates in the 2QCMC-HA-PEG (36.51 ± 7.93 %) and 2QCMC-HA-PEG@MnO_2 (40.25 ± 6.95 %) groups were significantly higher than those in the control (10.26 ± 2.04 %) and CMC-PEG (23.67 ± 8.63 %) groups (Fig. 8C). This could be attributed to the addition of quaternary ammonium salts and HA, which have hemostatic and antibacterial effects in the early stage of wound healing. On day 7 and 14, wounds treated with 2QCMC-HA-PEG@MnO_2 have a higher wound closure rate (74.24 ± 5.58 % and 95.98 ± 1.57 %) than that of control (55.44 ± 6.13 % and 79.21 ± 5.47 %), CMC-PEG (63.87 ± 5.83 % and 84.81 ± 3.22), and 2QCMC-HA-PEG (68.54 ± 5.12 % and 92.17 ± 1.93 %) groups. Therefore, the results reveal that the treating effect of 2QCMC-HA-PEG@MnO_2 was better than that of 2QCMC-HA-PEG,

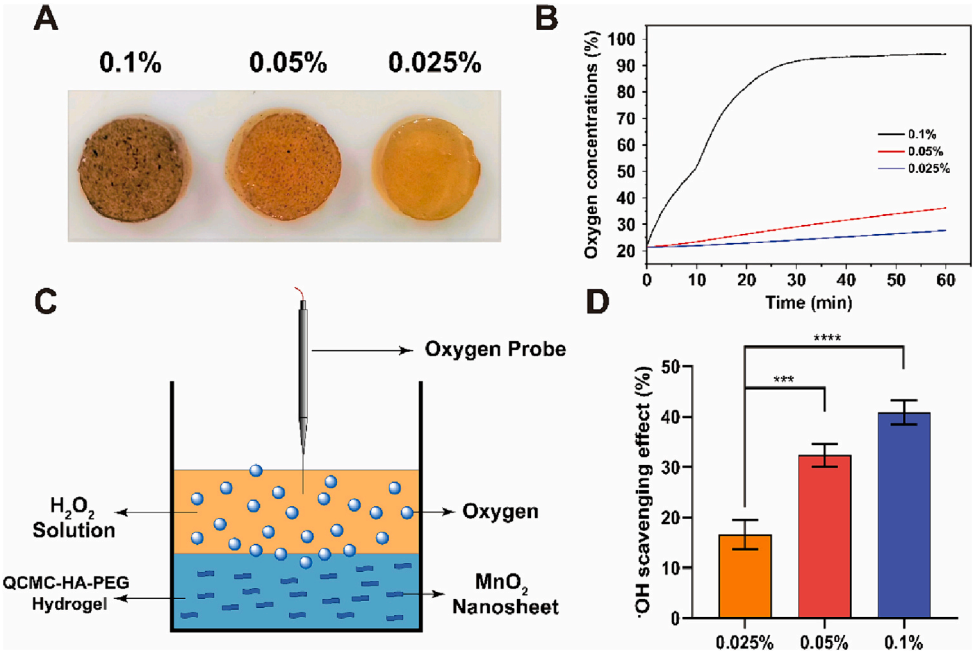

Fig. 6. (A) Hydrogels with different concentrations MnO_2 nanosheets; (B) the real-time O_2 level monitored by an oxygen probe; (C) schematic diagram of oxygen production performance of hydrogels; (D) the hydroxyl radical scavenging effects of different 2QCMC-HA-PEG@MnO_2 hydrogels. ($n = 3$, ***$p < 0.001$ and ****$p < 0.0001$.)

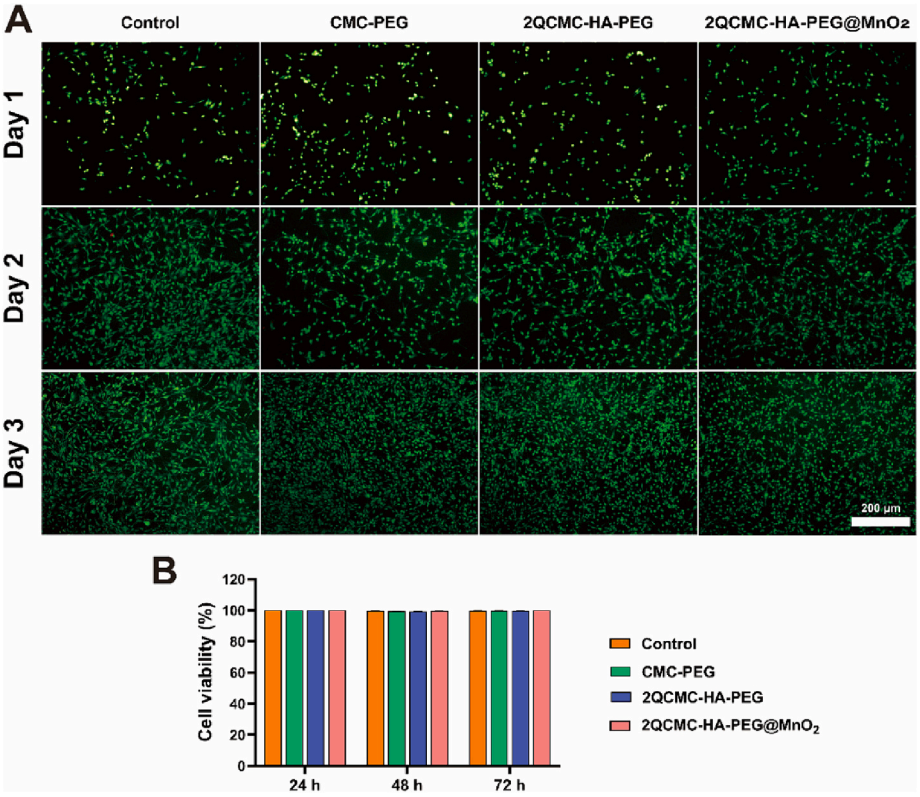

Fig. 7. (A) The LIVE/DEAD fluorescence images at day 1, 2, and 3 with different treatments; (B) NIH3T3 cells viability on day 1, 2, and 3 analyzed by LIVE/DEAD cytotoxicity assay.

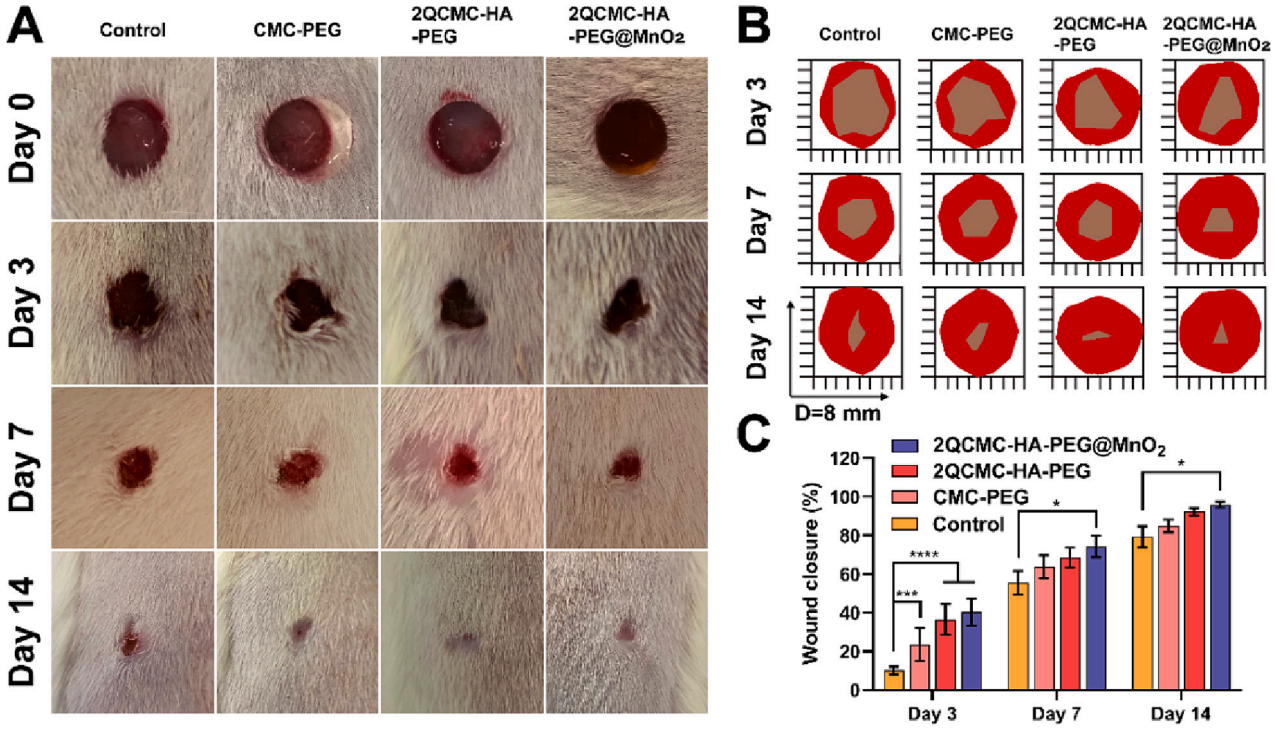

Fig. 8. (A) Representative photographs of cutaneous wounds treated by hydrogels on day 0, 3, 7, and 14; (B) area traces of wound closure over 14 days after therapy; (C) wound closure rates of all groups on day 3, 7, and 14. ($n = 4$, $^{*}p < 0.05$, $^{***}p < 0.001$, and $^{****}p < 0.0001$.)

attributing to the loading of MnO_2 nanosheets. Because the loaded MnO_2 nanosheets could both scavenge active oxygen species and promote oxygen production to further facilitate cell proliferation. In addition, it is noticeable that the wound area of 2QCMC-HA-PEG@MnO_2 group was smaller than that of other groups within the range of day 3 to day 14. Because the MnO_2 nanosheets evenly distributed in the hydrogel and

played oxygen production effect durably and uniformly. What's more, higher wound closure rates of 2QCMC-HA-PEG and 2QCMC-HA-PEG@MnO_2 could be observed on day 14 than that of CMC-PEG, attributing to the angiogenic property of HA. Because the property plays a vital role in promoting re-epithelialization and shortening the period of wound healing. Overall, the results above demonstrate that the 2QCMC-HA-PEG@MnO_2 hydrogel holds promising potential for expediting the wound healing process.

3.8. H&E and Masson staining

Fig. 9A shows that new epithelial and granulation tissues have appeared after 7-day treatments. As shown in Fig. 9C, the thickness of the neonatal epithelium in the 2QCMC-HA-PEG group (165.2 ± 46.25 μm) and the 2QCMC-HA-PEG@MnO_2 group (152.2 ± 35.42 μm) was significantly higher than that in the control group (94.21 ± 15.18 μm) and CMC-PEG (96.8 ± 131.31 μm). After the inflammatory phase, capillary buds infiltrate the wound site and form granulation tissues with fibroblasts and endothelial cells to provide nutrients and oxygen for cell metabolism. Compared with the control group and the CMC-PEG group, the 2QCMC-HA-PEG and 2QCMC-HA-PEG@MnO_2 group had a higher number of newly formed blood vessels in the skin tissue (Fig. 9D), which may be attributed to the fact that HA can stimulate angiogenesis. The incorporation of MnO_2 nanosheets serves to eliminate excess ROS and mitigate the formation of hydroxyl radicals, thereby playing a crucial role in preventing ROS-induced damage to cellular structures and lipid peroxidation. These results suggest that the 2QCMC-HA-PEG@MnO_2 hydrogel not only has a protective effect on the wound surface but also can promote angiogenesis through the biological activity of HA [42], effectively promoting the re-epithelialization of the wound and accelerating wound healing.

As shown in Fig. 9B–E, Masson trichrome stain analysis of the group treated with 2QCMC-HA-PEG@MnO_2 revealed more densely packed collagen bundles compared with the other groups (control: 0.57 ± 0.06; CMC-PEG: 0.61 ± 0.02; 2QCMC-HA-PEG: 0.66 ± 0.04; 2QCMC-HA-PEG@MnO_2: 0.74 ± 0.05). 2QCMC-HA-PEG@MnO_2 group showed significantly higher collagen indices compared to the CMC-PEG group. On the 14th day, there was still a lot of granulation tissue in the skin of the control group, indicating that its healing speed was slower, while hair follicles had already been generated in the hydrogel group. Among them, the 2QCMC-HA-PEG@MnO_2 group had the best healing effect, and its structure was similar to normal skin. This is because nanoenzymes can scavenge excessive ROS and reduce the formation of hydroxyl free radicals, playing an important role in preventing excessive ROS from damaging cell structure, producing lipid peroxidation, and causing skin aging (Fig. S11). The results confirm that 2QCMC-HA-PEG@MnO_2 could promote epidermal regeneration and collagen regeneration during wound healing.

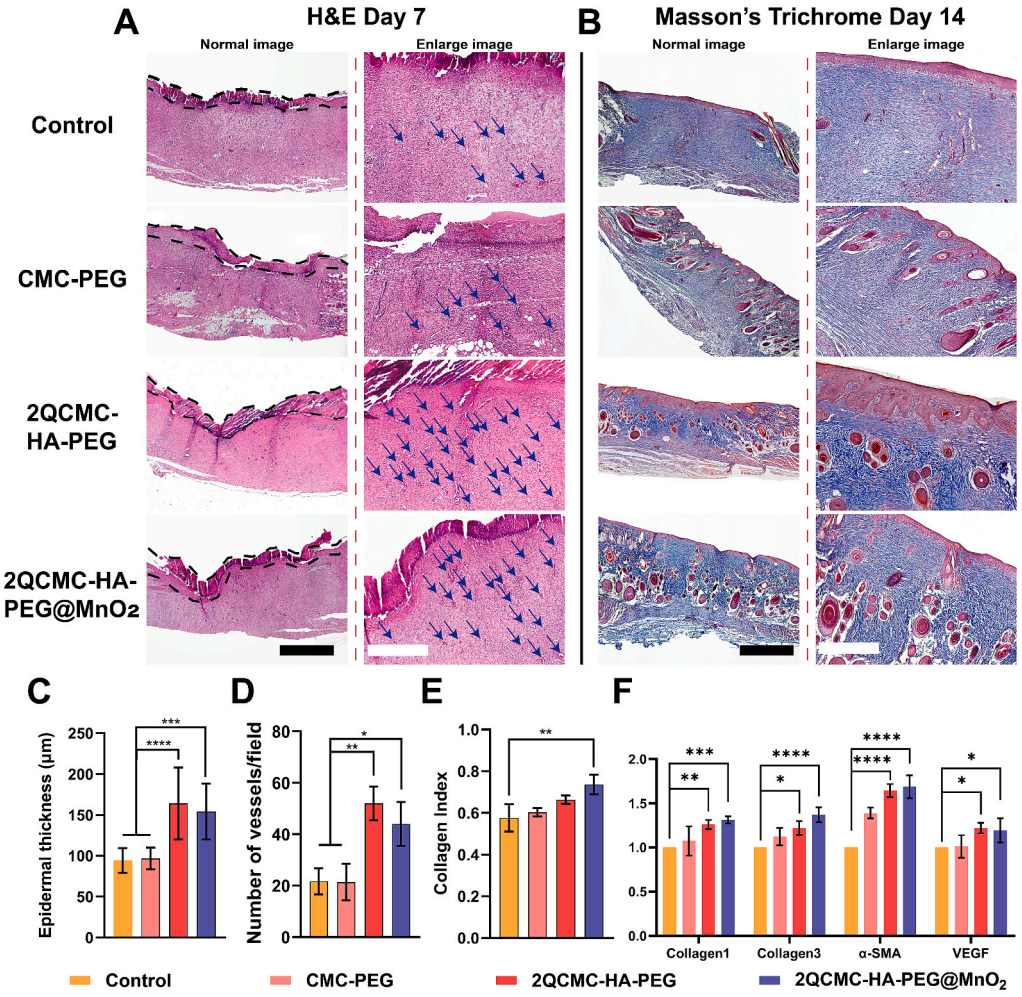

Fig. 9. (A) H&E staining and partially enlarged images of wound tissue on day 7 (black scale bar: 500 μm, white scale bar: 200 μm). The epidermis is represented by the dotted lines, and the granulation tissue is represented by the blue arrows; (B) Masson staining and partially enlarged images of wound tissue after surgery on day 14; (C) quantification of the epithelium thickness on day 7; (D) the number of blood vessels on day 7; (E) quantification of the collagen index on day 14; (F) The gene (Collagen-1, Collagen-3, α-SMA and VEGF) expression level of skin regeneration tissue on day 14. ($n = 3$, $^*p < 0.05$, $^{**}p < 0.01$, $^{***}p < 0.001$ and $^{****}p < 0.0001$.)

In terms of tissue remodeling, we focused on collagen deposition, muscle tissue regeneration, and vascularization to determine the mechanism and evaluate the intended effect. On day 14, the expression level of Collagen-1 and Collagen-3 in the regenerated skins was detected with qPCR, because they are the major components of skin collagen [43]. As the results showed in Fig. 9F, the expression level of Collagen-1 and Collagen-3 in 2QCMC-HA-PEG@MnO_2 group was the highest among all the groups. Reportedly [44], the expression of α-SMA in smooth muscle cells plays an important role in regulating the contraction and relaxation of cells and controlling the function and morphology of organs. Therefore, the expression level of α-SMA in the regenerated skins was further detected by qPCR on day 14. According to the results in Fig. 9F, the α-SMA expression level of 2QCMC-HA-PEG and 2QCMC-HA-PEG@MnO_2 groups was higher than that of control and CMC-PEG groups. In addition, the 2QCMC-HA-PEG@MnO_2 group had the highest expression level of α-SMA among all the groups. As previous studies reported [45], VEGF is one of the key regulators of angiogenesis, helping to form new vascular networks and promoting blood supply to tissues. Similarly, the expression level of VEGF in the regenerated skins was also detected by qPCR on day 14. According to the outcomes in Fig. 9F, the VEGF expression level of 2QCMC-HA-PEG and 2QCMC-HA-PEG@MnO_2 groups was higher than that of control and CMC-PEG groups, which was consistent with the quantification results of H&E. In conclusion, the 2QCMC-HA-PEG@MnO_2 hydrogel can significantly raise the expression level of collagen, α-SMA, and VEGF across the wound healing to facilitate the collagen deposition, muscle tissue regeneration, and vascularization.

3.9. Inflammatory factor expression

As an important pathophysiological response, inflammation has been proved to play a critical role in the process of wound healing [46]. Exhibiting pro-inflammatory functions, M1 macrophages can promote immune response in the early stages of skin wound healing, and kill foreign pathogens and bacteria. Having anti-inflammatory functions, M2 macrophages are mainly involved in tissue repairing in the later stages of wound recovery. Additionally, CD80 is a specific surface marker for M1 macrophages. After surgical treatments for 2 weeks, the expression level of CD80 of control group was higher than that of CMC-PEG, 2QCMC-HA-PEG, and 2QCMC-HA-PEG@MnO_2 groups, as shown in Fig. 10A and B. What's more, CD206 is a biomarker of selectively activated inflammatory cells associated with anti-inflammatory and tissue remodeling responses. As shown in Fig. 10A–C, the expression level of CD206 of 2QCMC-HA-PEG and 2QCMC-HA-PEG@MnO_2 groups was significantly higher than that of control group, which could be attributed to the anti-inflammatory ability of HA.

Macrophages can be divided into pro-inflammatory phenotype and anti-inflammatory phenotype. Pro-inflammatory macrophages mainly secrete pro-inflammatory factors such as iNOS, IL-6, IL-1β, and TNF-α, while anti-inflammatory macrophages mainly secrete ARG-1, TGF-β, IL-10, and other anti-inflammatory factors. Thus, after treatments for 2 weeks, we used qPCR to detect the expression level of major inflammatory factors in 2QCMC-HA-PEG@MnO_2 treated group to further verify the phenotypic transformation of macrophages. According to the results in Fig. 10D–E, the expression level of anti-inflammatory factors such as ARG-1, TGF-β and IL-10 in 2QCMC-HA-PEG@MnO_2 group was lower than that of other groups, while the expression level of pro-inflammatory factors such as iNOS, IL-6, IL-1β was opposite. These outcomes indicate that the 2QCMC-HA-PEG@MnO_2 hydrogel exhibited anti-inflammatory capacity via regulating the transformation of macrophages from M1 to M2 during the tissue-remodeling stage.

4. Conclusion

In conclusion, although the 2QCMC-HA-PEG@MnO_2 exhibited certain limitations in hemostasis, we have successfully developed a hybrid hydrogel with excellent antibacterial and self-healing properties and good adhesion for promoting wound healing. The results show that the hydrogel had good performance in the ROS scavenging experiment in vitro and exhibited a sustained oxygen production effect across the experimental process. Therefore, it was able to kill bacteria and promote cell proliferation in the early stage of wound healing. Moreover, the 2QCMC-HA-PEG@MnO_2 hydrogel performed better than other groups in promoting angiogenesis, collagen deposition, inflammatory regulation, and epidermal regeneration, according to the outcomes of the full-layer wound repairing experiment and qPCR quantitative analysis results. In summary, the designed hydrogel has great potential to be used as skin wound dressing in the applications of biomedical fields.

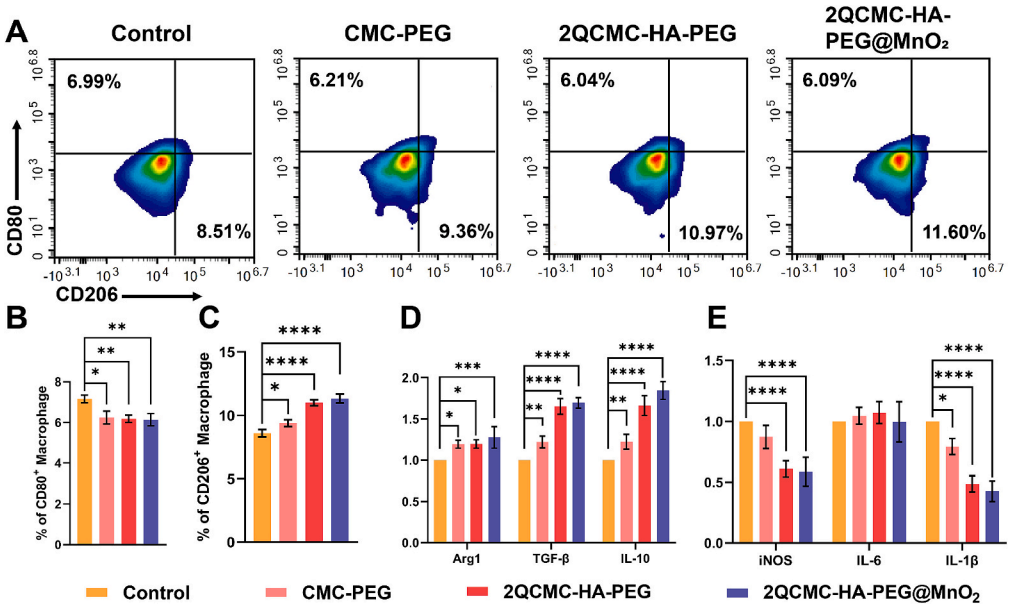

Fig. 10. (A) Flow cytometry analysis of wound tissue on day 14; (B) flow cytometry analysis of M1 macrophage infiltration at skin wound tissue; (C) flow cytometry analysis of M2 macrophage infiltration at skin wound tissue; (D) expression level of anti-inflammatory factors in wound tissue on day 14; (E) expression level of pro-inflammatory factors in wound tissue on day 14. ($n = 3$, $^{*}p < 0.05$, $^{**}p < 0.01$, $^{***}p < 0.001$ and $^{****}p < 0.0001$.)

CRediT authorship contribution statement

Yahao Ma: Writing – review & editing, Validation, Methodology, Investigation, Formal analysis, Data curation, Conceptualization. **Xujie Zhou:** Validation, Methodology, Investigation, Formal analysis, Data curation, Conceptualization, Writing – review & editing. **Zhendong Mo:** Formal analysis, Investigation, Validation. **Qing Zhou:** Formal analysis, Investigation, Validation. **Bingyu Hui:** Investigation, Formal analysis. **Zhuangzhuang Cai:** Investigation, Formal analysis. **Xiaoying Wang:** Writing – review & editing, Project administration. **Hang Li:** Writing – review & editing, Supervision, Resources, Project administration, Funding acquisition. **Shunqing Tang:** Writing – review & editing, Supervision, Project administration, Funding acquisition, Resources.

Declaration of competing interest

The authors declare no competing interests.

Data availability

Data will be made available on request.

Acknowledgments

This work was financially supported by the National Natural Science Foundation of China (32171312), Guangdong Basic and Applied Basic Research Foundation (2020A1515110771), the Innovation and Entrepreneurship Training Program for Undergraduate (CX22417), and the Key Areas Research and Development Program of Guangzhou (202103030003, 2023b03j1241).

Appendix A. Supplementary data

Supplementary data to this article can be found online at https://doi.org/10.1016/j.ijbiomac.2024.131871.

References

[1] A.A. Nash, R.G. Dalziel, J.R. Fitzgerald, Mims' Pathogenesis of Infectious Disease, Academic Press, 2015.
[2] J.A. Plumb, L.A. Hanson, Health Maintenance and Principal Microbial Diseases of Cultured Fishes, John Wiley & Sons, 2010.
[3] A. Farazin, Z. Torkpour, S. Dehghani, R. Mohammadi, M.D. Fahmy, et al., A review on polymeric wound dress for the treatment of burns and diabetic wounds, Int. J. Basic Sci. Med. 6 (2021) 44–50, https://doi.org/10.34172/ijbsm.2021.08.
[4] J.S. Boateng, K.H. Matthews, H.N. Stevens, G.M. Eccleston, Wound healing dressings and drug delivery systems: a review, J. Pharm. Sci. 97 (2008) 2892–2923, https://doi.org/10.1002/jps.21210.
[5] X. Ding, G. Li, P. Zhang, et al., Injectable self-healing hydrogel wound dressing with cysteine-specific on-demand dissolution property based on tandem dynamic covalent bonds, Adv. Funct. Mater. 31 (2021) 2011230, https://doi.org/10.1002/adfm.202011230.
[6] Q. Zong, X. Peng, Y. Ding, H. Wu, et al., Multifunctional hydrogel wound dressing with rapid on-demand degradation property based on aliphatic polycarbonate and chitosan, Int. J. Biol. Macromol. (2023) 125138, https://doi.org/10.1016/j.ijbiomac.2023.125138.
[7] H.A. Heydary, E. Karamian, E. Poorazizi, A. Khandan, et al., A novel nano-fiber of Iranian gum tragacanth-polyvinyl alcohol/nanoclay composite for wound healing applications, Procedia, Mater. Sci. 11 (2015) 176–182, https://doi.org/10.1016/j.mspro.2015.11.079.
[8] Z. Doozandeh, S. Saber-Samandari, A. Khandan, Preparation of novel Arabic gum-C_6H_9NO biopolymer as a bedsore for wound care application, Acta Med, Iran (2020) 520–530, https://doi.org/10.18502/acta.v58i10.4915.
[9] K.L. Goa, P. Benfield, Hyaluronic acid, Drugs 47 (1994) 536–566, https://doi.org/10.2165/00003495-199447030-00009.
[10] H. Hecht, S. Srebnik, Structural characterization of sodium alginate and calcium alginate, Biomacromolecules 17 (2016) 2160–2167, https://doi.org/10.1021/acs.biomac.6b00378.
[11] V.K. Mourya, N.N. Inamdar, Chitosan-modifications and applications: opportunities galore, React. Funct. Polym. 68 (2008) 1013–1051, https://doi.org/10.1016/j.reactfunctpolym.2008.03.002.
[12] Y. Hou, T. Tan, Z. Guo, Y. Ji, J. Hu, Y. Zhang, Gram-selective antibacterial peptide hydrogels, Biomater. Sci. 10 (2022) 3831–3844, https://doi.org/10.1039/d2bm00558a.
[13] L. Zhang, Y. Zhang, F. Ma, X. Liu, Y. Liu, et al., A low-swelling and toughened adhesive hydrogel with anti-microbial and hemostatic capacities for wound healing, J. Mater. Chem. B 10 (2022) 915–926, https://doi.org/10.1039/d1tb01871j.
[14] Z. Sao, W. Wang, Y. Wang, W. Zhao, C. Zhao, A burning grass and removing root immunoregulatory strategy toward chronic wounds therapy by MnO_2 nanoparticle incorporated hyaluronic acid hydrogel, Adv. Mater. Technol. 8 (2023) 2300669, https://doi.org/10.1002/admt.202300669.
[15] V.K. Mourya, N.N. Inamdara, A. Tiwari, Carboxymethyl chitosan and its applications, Adv. Mater. Lett. 1 (2010) 11–33, https://doi.org/10.5185/amlett.2010.3108.
[16] M.E. Abd El-Hack, M.T. El-Saadony, M.E. Shafi, N.M. Zabermawi, M. Arif, G. E. Batiha, A.F. Khafaga, Y.M. Abd El-Hakim, A.A. Al-Sagheer, Antimicrobial and antioxidant properties of chitosan and its derivatives and their applications: a review, Int. J. Biol. Macromol. 164 (2020) 2726–2744, https://doi.org/10.1016/j.ijbiomac.2020.08.153.
[17] J. Li, S.J.E.P.J. Zhuang, Antibacterial activity of chitosan and its derivatives and their interaction mechanism with bacteria: current state and perspectives, Eur. Polym. J. 138 (2020) 109984, doi:https://doi.org/10.1016/j.eurpolymj.2020.109984.
[18] A. Hui, R. Yan, W. Wang, Q. Wang, Y. Zhou, A.J.C.p. Wang, Incorporation of quaternary ammonium chitooligosaccharides on ZnO/palygorskite nanocomposites for enhancing antibacterial activities, Carbohydr. Polym. 247 (2020) 116685, doi:https://doi.org/10.1016/j.carbpol.2020.116685.
[19] U. Filipović, R.G. Dahmane, S. Ghannouchi, A. Zore, K.J.A.i.C. Bohinc, I. Science, Bacterial adhesion on orthopedic implants, Adv. Colloid Interface Sci. 283 (2020) 102228, doi:https://doi.org/10.1016/j.cis.2020.102228.
[20] G. Pan, F. Li, S. He, W. Li, Q. Wu, J. He, R. Ruan, Z. Xiao, J. Zhang, H.J.A.F.M. Yang, Mussel-and barnacle cement proteins-inspired dual-bionic bioadhesive with repeatable wet-tissue adhesion, multimodal self-healing, and antibacterial capability for nonpressing hemostasis and promoted wound healing, Adv. Funct. Mater. 32 (2022) 2200908, doi:https://doi.org/10.1002/adfm.202200908.
[21] Q. Xu, A. Sigen, Y. Gao, L. Guo, J. Creagh-Flynn, et al., A hybrid injectable hydrogel from hyperbranched PEG macromer as a stem cell delivery and retention platform for diabetic wound healing, Acta Biomater. 75 (2018) 63–74, https://doi.org/10.1016/j.actbio.2018.05.039.
[22] H. Li, X. Zhou, L. Luo, Q. Ding, S. Tang, Bio-orthogonally crosslinked catechol–chitosan hydrogel for effective hemostasis and wound healing, Carbohydr. Polym. 281 (2022) 119039, https://doi.org/10.1016/j.carbpol.2021.119039.
[23] C. Dunnill, T. Patton, J. Brennan, J. Barrett, M. Dryden, J. Cooke, D. Leaper, N. T. Georgopoulos, Reactive oxygen species (ROS) and wound healing: the functional role of ROS and emerging ROS-modulating technologies for augmentation of the healing process, Int. Wound J. 14 (2017) 89–96, https://doi.org/10.1111/iwj.12557.
[24] S. Wang, H. Zheng, L. Zhou, F. Cheng, Z. Liu, H. Zhang, L. Wang, Q. Zhang, Nanoenzyme-reinforced injectable hydrogel for healing diabetic wounds infected with multidrug resistant bacteria, Nano Lett. 20 (2020) 5149–5158, https://doi.org/10.1021/acs.nanolett.0c01371.
[25] S. Wang, H. Zheng, L. Zhou, F. Cheng, Z. Liu, H. Zhang, Q.J.B. Zhang, Injectable redox and light responsive MnO_2 hybrid hydrogel for simultaneous melanoma therapy and multidrug-resistant bacteria-infected wound healing, Biomaterials 260 (2020) 120314, https://doi.org/10.1016/j.biomaterials.2020.120314.
[26] S. Schreml, R. Szeimies, L. Prantl, S. Karrer, M. Landthaler, P. Babilas, Oxygen in acute and chronic wound healing, Br. J. Dermatol. 163 (2010) 257–268, https://doi.org/10.1111/j.1365-2133.2010.09804.x.
[27] C. Li, X. He, Q. Li, M. Lv, J. Shen, L. Jin, D.J.N.A.M. He, A photothermal-response oxygen release platform based on a hydrogel for accelerating wound healing, NPG Asia Mater. 15 (2023) 3, doi:https://doi.org/10.1038/s41427-022-00456-7.
[28] E. Neyens, J.J. Baeyens, A review of classic Fenton's peroxidation as an advanced oxidation technique, J. Hazard. Mater. 98 (2003) 33–50, https://doi.org/10.1016/s0304-3894(02)00282-0.
[29] Y. Li, H. Yang, X. Zong, X. Li, P. Yuan, C. Yang, X. Chen, X. Yan, Y. Wen, T. Zhu, W. Xue, J. Dai, Oncolytic virus-like nanoparticles for tumor-specific gene delivery, Adv. Funct. Mater. (2024) 2314898, https://doi.org/10.1002/adfm.202314898.
[30] L. Xiao, P. Xie, J. Ma, K. Shi, Y. Dai, M. Pang, J. Luo, Z. Tan, Y. Ma, X. Wang, L. Rong, L. He, A bioinspired injectable, adhesive, and self-healing hydrogel with dual hybrid network for neural regeneration after spinal cord injury, Adv. Mater. 35 (2023) 2304896, https://doi.org/10.1002/adma.202304896.
[31] T. Zhai, Y.-C. Chang, Standing of environmental public-interest litigants in China: evolution, obstacles and solutions, J. Environ. Law 30 (2018) 369–397, https://doi.org/10.1093/jel/eqy011.
[32] N. Chehl, G. Chipitsyna, Q. Gong, C.J. Yeo, H.A.J.H. Arafat, Anti-inflammatory effects of the Nigella sativa seed extract, thymoquinone, in pancreatic cancer cells, Hpb 11 (2009) 373–381, https://doi.org/10.1111/j.1477-2574.2009.00059.x.
[33] H.-C. Ge, D.-K. Luo, Preparation of carboxymethyl chitosan in aqueous solution under microwave irradiation, Carbohydr. Res. 340 (2005) 1351–1356, https://doi.org/10.1016/j.carres.2005.02.025.
[34] L. Sun, Y. Du, L. Fan, X. Chen, J.J.P. Yang, Preparation, characterization and antimicrobial activity of quaternized carboxymethyl chitosan and application as pulp-cap, Polymer 47 (2006) 1796–1804, https://doi.org/10.1016/j.polymer.2006.01.073.
[35] S. Huang, J. Wang, Y. Zhang, Z. Yu, C.J.N. Qi, Quaternized carboxymethyl chitosan-based silver nanoparticles hybrid: microwave-assisted synthesis, characterization and antibacterial activity, Nanomaterials 6 (2016) 118, https://doi.org/10.3390/nano6060118.

[36] J.K. Kim, P. Srinivasan, J.H. Kim, J.I. Choi, H.J. Park, M.W. Byun, J.W. Lee, Structural and antioxidant properties of gamma irradiated hyaluronic acid, Food Chem. 109 (4) (2008) 763–770, https://doi.org/10.1016/j.foodchem.2008.01.038.
[37] L.H. Toledo-Pereyra, F. Lopez-Neblina, A.H.J.A. Toledo, Reactive oxygen species and molecular biology of ischemia/reperfusion, Ann. Transplant. 9 (2004) 81–83.
[38] L. Li, B. Xiao, J. Mu, Y. Zhang, C. Zhang, H. Cao, R. Chen, H.K. Patra, B. Yang, S. Feng, A MnO_2 nanoparticle-dotted hydrogel promotes spinal cord repair via regulating reactive oxygen species microenvironment and synergizing with mesenchymal stem cells, ACS Nano 13 (2019) 14283–14293, https://doi.org/10.1021/acsnano.9b07598.
[39] Z. Jia, W. Xu, Synthesis and antibacterial activities of quaternary ammonium salt of chitosan, Carbohydr. Res. 333 (2001) 1–6.
[40] M.R. Kumar, R.A. Muzzarelli, C. Muzzarelli, H. Sashiwa, A. Domb, Chitosan chemistry and pharmaceutical perspectives, Chem. Rev. 104 (2004) 6017–6084, https://doi.org/10.1021/cr030441b.
[41] A. Kalra, A. Lowe, A.J.J.M.S.E. Al-Jumaily, Mechanical behaviour of skin: a review, J. Mater. Sci. Eng. 5 (2016) 1000254, doi:https://doi.org/10.4172/2169-0022.1000254.
[42] J. Voigt, V.R. Driver, Hyaluronic acid derivatives and their healing effect on burns, epithelial surgical wounds, and chronic wounds: a systematic review and meta-analysis of randomized controlled trials, Wound Repair Regen. 20 (2012) 317–331, https://doi.org/10.1111/j.1524-475x.2012.00777.x.
[43] M.G. Patino, M.E. Neiders, S. Andreana, B. Noble, R.E. Cohen, Collagen: an overview, Implant. Dent. 11 (2002) 280–285, https://doi.org/10.1097/00008505-200207000-00014.
[44] S.S.M. Rensen, P.A.F.M. Doevendans, G.J.J.M. Van Eys, Regulation and characteristics of vascular smooth muscle cell phenotypic diversity, Neth. Hear. J. 15 (2007) 100–108, https://doi.org/10.1007/bf03085963.
[45] K.E. Johnson, T.A. Wilgus, Vascular endothelial growth factor and angiogenesis in the regulation of cutaneous wound repair, Adv. Wound Care 3 (2014) 647–661, https://doi.org/10.1089/wound.2013.0517.
[46] T.J. Koh, L.A. DiPietro, Inflammation and wound healing: the role of the macrophage, Expert Rev. Mol. Med. 13 (2011) e23, https://doi.org/10.1017/S1462399411001943.